Optimization of shunted piezoelectric patches for vibration reduction of complex structures - Application to a turbojet fan blade

Aurélien Sénéchal, Olivier Thomas, Jean-François Deü

OPTIMIZATION OF SHUNTED PIEZOELECTRIC PATCHES FOR VIBRATION REDUCTION OF COMPLEX STRUCTURES - APPLICATION TO A TURBOJET FAN BLADE

Aurélien Sénéchal,* Olivier Thomas, Jean François Deü
Structural Mechanics and Coupled System Laboratory
Chaire de Mécanique du Cnam
case courrier 353,
2 rue Conté, 75003 Paris, France
Email: aurelien.senechal@cnam.fr

1 INTRODUCTION

Vibration reduction of a turbojet fan blade with piezoelectric patches connected to a passive electrical circuit, commonly called "shunt", is addressed in this study. The purpose of this work is to present a method for maximizing the performance of a piezoelectric resonant shunt. The cases of resistive shunt [1] and switch techniques [2] are not covered here but the method remains valid.

To improve the damping level, a key issue is the optimization of the whole system, in terms of location and size of the piezoelectric patches and electric circuit components choice. It was shown in [3] these two optimizations, mechanical and electrical, can be realized separately. Moreover, it is proved in [1, 4–6] that the only parameters to maximize are the modal electromechanical coupling factors (MEMCF), which characterize the energy exchanges between the mechanical structure and the piezoelectric patches for a given mode. Since the optimal value of the electric circuit parameters are known as functions of the MEMCF and the system structural characteristics [3, 7], they can be evaluated in a second step. Thus, the mechanical optimization consists in maximizing the MEMCF by optimizing the patches positions and dimensions, *i.e.* finding the best design. To fulfill this requirement and in order to manage a complex geometry, a 3D finite element (FE) formulation of the coupled electromechanical problem is derived [8]. A reduced order model of the discretized problem is then obtained by expanding the mechanical displacement unknowns vector onto the short-circuit eigenmodes to get the MEMCF.

However, when the optimization aims to reduce the vibration level with several patches, the main concern arises from the huge number of possible designs to test. Finding the optimal design without a strategy is simply impossible within a reasonable amount of time. Even when the size of the search space is reduced, *i.e.* some design parameters are fixed, it remains a very time consuming approach since for each design, an elastic mechanical problem have to be solved to compute the MEMCF. For that reason, a method is proposed to cut back the simulations time span as well as to cope with the many local minima. This method consists in splitting up the optimization procedure in two steps. In the first one, the influence of patches on the structural eigenmodes is neglected, which is equivalent to say the patches have a negligible thickness. Therefore, an analytic coupling indicator, based on the modes of the naked structure, is defined and gives rise to a first approximate optimization using a simulated annealing algorithm [9–12]. Then, the solutions of the first step are used as a starting point for a second optimization, working with the tabu search algorithm [12–15] and where the stiffness and the mass of the patches are taken into account.

*Address all correspondence to this author.

2 FINITE ELEMENT MODEL

In this section, the general formulation of the equations that govern the mechanical and electrical state of an elastic structure equipped with piezoelectric patches is used to derive a finite element model [5, 8, 16]. Beforehand, the general problem is described and the main assumptions are recalled.

2.1 Hypotheses and Variational Formulation

An elastic structure, occupying a domain denoted Ω_s, is equipped with P piezoelectric patches. Each piezoelectric patch has its upper and lower surfaces covered with a very thin electrode and can be slightly curved. The p-th patch, $p \in \{1, \cdots, P\}$, occupies a domain $\Omega^{(p)}$ such that $\left(\Omega_s, \Omega^{(1)}, \cdots, \Omega^{(P)}\right)$ is a partition of the whole domain Ω. The domain Ω is subjected to prescribed body forces f_i^d and the domain boundary, denoted $\partial\Omega$, is subjected to a prescribed displacement u_i^d on a part Γ_u and to a prescribed surface force density t_i^d on the complementary part Γ_t, such that $\partial\Omega = \Gamma_u \cup \Gamma_t$.

A set of hypotheses, applicable to a wide spectrum of practical applications, can be used in order to obtain an efficient variational formulation of the problem. The main assumptions, detailed in [8], are summarized below.

- Only the piezoelectric patches are made of piezoelectric material. Consequently, the piezoelectric material constants e_{ijk} vanish in Ω_s. The electric displacement vector of component D_i is neglected in the elastic domain Ω_s, as compared to its value in any of the piezoelectric patches $\Omega^{(p)}$.
- The piezoelectric patches are thin with a constant thickness, denoted $h^{(p)}$ for the p-th patch, smaller than its characteristic longitudinal length. The thickness of the electrodes is much smaller than $h^{(p)}$ and is thus neglected.
- The piezoelectric patches are polarized in their transverse direction (*i.e.* the direction normal to the electrodes). Moreover, the electric field vector, of components E_k, is normal to the electrodes and uniform in the piezoelectric patch, so that for all $p \in \{1, \ldots, P\}$

$$E_k = -\frac{V^{(p)}}{h^{(p)}} n_k, \quad \text{in } \Omega^{(p)}, \tag{1}$$

where $V^{(p)} = \psi_+^{(p)} - \psi_-^{(p)}$ is the potential difference between the p-th patch upper and lower electrodes surfaces $\Gamma_+^{(p)}$ and $\Gamma_-^{(p)}$ and n_k is the k-th component of the normal unit vector to the surface of the electrodes.

Considering the above hypotheses, it can be shown that the variational formulation of the electromechanical problem is such that

$$\int_\Omega c_{ijkl}\varepsilon_{kl}(u)\varepsilon_{ij}(\delta u)\,\mathrm{d}\Omega + \sum_{p=1}^{P} \frac{V^{(p)}}{h^{(p)}} \int_{\Omega^{(p)}} e_{kij} n_k \varepsilon_{ij}(\delta u)\,\mathrm{d}\Omega + \int_\Omega \rho \frac{\partial^2 u_i}{\partial t^2}\,\delta u_i\,\mathrm{d}\Omega = \int_\Omega f_i^d\,\delta u_i\,\mathrm{d}\Omega + \int_{\Gamma_t} t_i^d\,\delta u_i\,\mathrm{d}S \quad \forall \delta u_i \in \mathcal{C}_u^*, \tag{2}$$

and

$$-\sum_{p=1}^{P} \frac{\delta V^{(p)}}{h^{(p)}} \int_{\Omega^{(p)}} e_{ikl}\varepsilon_{kl}(u) n_i\,\mathrm{d}\Omega + \sum_{p=1}^{P} \delta V^{(p)} C^{(p)} V^{(p)} = \sum_{p=1}^{P} \delta V^{(p)} Q^{(p)} \quad \forall \delta V^{(p)} \in \mathbb{R}, \tag{3}$$

where $C^{(p)} = \epsilon_{33}\Omega^{(p)}/(h^{(p)})^2$ is the capacitance of the p-th piezoelectric patch ($\epsilon_{33} = \epsilon_{ik} n_i n_k$ being the piezoelectric permittivity in the direction normal to the electrodes) and $Q^{(p)}$ the electric charge contained in the upper electrode of the p-th piezoelectric patch.

For more details about the derivation of this original formulation, we refer the reader to [8]. It can be noted that we have defined $\mathcal{C}_u$ as the space of sufficiently regular functions u_i defined in the whole domain Ω and $\mathcal{C}_u^* = \{u_i \in \mathcal{C}_u \mid u_i = 0 \text{ on } \Gamma_u\}$.

2.2 Finite Element Formulation

Using the finite element method to discretize the mechanical part of equations Eq. (2) and Eq. (3) leads to the following matrices definitions:

$$\int_\Omega \rho \frac{\partial^2 u_i}{\partial t^2} \delta u_i\,\mathrm{d}\Omega \quad \Longrightarrow \quad \delta\mathbf{U}^{\mathrm{T}}\mathbf{M}_m\mathbf{U}, \tag{4}$$

$$\int_\Omega c_{ijkl}\varepsilon_{kl}(u)\varepsilon_{ij}(\delta u)\,\mathrm{d}\Omega \quad \Longrightarrow \quad \delta\mathbf{U}^{\mathrm{T}}\mathbf{K}_m\mathbf{U}, \tag{5}$$

$$\sum_{p=1}^{P} \frac{V^{(p)}}{h^{(p)}} \int_{\Omega^{(p)}} e_{kij} n_k \varepsilon_{ij}(\delta u)\,\mathrm{d}\Omega \quad \Longrightarrow \quad \delta\mathbf{U}^{\mathrm{T}}\mathbf{K}_c\mathbf{V}, \tag{6}$$

$$\sum_{p=1}^{P} \delta V^{(p)} C^{(p)} V^{(p)} \quad \Longrightarrow \quad \delta\mathbf{V}^{\mathrm{T}}\mathbf{K}_e\mathbf{V}, \tag{7}$$

$$\int_\Omega f_i^d \delta u_i\,\mathrm{d}\Omega + \int_{\Gamma_t} t_i^d \delta u_i\,\mathrm{d}S \quad \Longrightarrow \quad \delta\mathbf{U}^{\mathrm{T}}\mathbf{F}, \tag{8}$$

$$\sum_{p=1}^{P} \delta V^{(p)} Q^{(p)} \quad \Longrightarrow \quad \delta\mathbf{V}^{\mathrm{T}}\mathbf{Q}, \tag{9}$$

with $\mathbf{U}$ the vector of nodal values of u_i, $\mathbf{Q} = \left(Q^{(1)}Q^{(2)}\cdots Q^{(P)}\right)^{\mathrm{T}}$ the column vector of electric charges and $\mathbf{V} = \left(V^{(1)}V^{(2)}\cdots V^{(P)}\right)^{\mathrm{T}}$ the column vector of potential differences. $\mathbf{M}_m$ and $\mathbf{K}_m$ are the mechanical mass and stiffness matrices, of size $N \times N$, where N is the number of mechanical degrees of freedom (dof). $\mathbf{K}_c$ is the electromechanical coupling matrix, of size $N \times P$. $\mathbf{K}_e = \mathrm{diag}\left(C^{(1)}\cdots C^{(P)}\right)$ is the diagonal matrix filled with the P capacitances of the piezoelectric patches. $\mathbf{F}$ is the column vector of mechanical forcing, of length N. The general finite element formulation of the electromechanical problem can be written in the following matrix form

$$\begin{pmatrix}\mathbf{M}_m & \mathbf{0}\\ \mathbf{0} & \mathbf{0}\end{pmatrix}\begin{pmatrix}\ddot{\mathbf{U}}\\ \ddot{\mathbf{V}}\end{pmatrix} + \begin{pmatrix}\mathbf{K}_m & \mathbf{K}_c\\ -\mathbf{K}_c^T & \mathbf{K}_e\end{pmatrix}\begin{pmatrix}\mathbf{U}\\ \mathbf{V}\end{pmatrix} = \begin{pmatrix}\mathbf{F}\\ \mathbf{Q}\end{pmatrix}. \tag{10}$$

The above discretized formulation Eq. (10) is particularly adapted when the piezoelectric patches are "shunted", that is to say, connected to a passive electrical network. In this case, neither $\mathbf{V}$ nor $\mathbf{Q}$ are prescribed by the electrical network but the latter imposes only a relation between them. For a resonant shunt connected to the p-th patch and composed of a resistance R and an inductance L [8, 17], one obtains

$$V^{(p)} - L\ddot{Q}^{(p)} - R\dot{Q}^{(p)} = 0. \tag{11}$$

Depending on whether the patches are short-circuited ($\mathbf{V} = \mathbf{0}$) or in open-circuit ($\mathbf{Q} = \mathbf{0}$), the homogeneous problem associated to the discretized formulation (10) takes the following forms:

$$\mathbf{M}_m\ddot{\mathbf{U}} + \mathbf{K}_m\mathbf{U} = \mathbf{0} \quad \text{short-circuit,} \tag{12}$$

$$\mathbf{M}_m\ddot{\mathbf{U}} + \left(\mathbf{K}_m + \mathbf{K}_c\mathbf{K}_e^{-1}\mathbf{K}_c^{\mathrm{T}}\right)\mathbf{U} = \mathbf{0} \quad \text{open-circuit.} \tag{13}$$

Therefore, one can notice the effect of open-circuit electromechanical coupling on the elastic structure appears as an added stiffness term $\mathbf{K}_c\mathbf{K}_e^{-1}\mathbf{K}_c^{\mathrm{T}}$.

2.3 Modal Expansion and Coupling Coefficient

In this section, a reduced-order formulation of the discretized problem is derived by expanding the mechanical displacement unknowns vector onto the short-circuit eigenmodes basis. The coupling factors are also introduced.

2.3.1 Short-circuit Eigenmodes

The natural angular frequencies ω_i and mode shapes $\mathbf{\Phi}_i$ of the short-circuited system (Eq. (12)) are the N eigensolutions of the following problem

$$\mathbf{K}_m\mathbf{\Phi} - \omega^2\mathbf{M}_m\mathbf{\Phi} = \mathbf{0}, \tag{14}$$

which depends only on the mechanical properties of the system, *i.e.* the stiffness and mass of the structure and patches. In addition, the modes verify the orthogonality properties and are normalized with respect to the mass matrix: $\mathbf{\Phi}^{\mathrm{T}}\mathbf{M}_m\mathbf{\Phi} = \mathbf{1}$.

2.3.2 Modal Expansion

The mechanical displacement vector is sought as: $\mathbf{U}(t) = \sum_{i=1}^{N}\mathbf{\Phi}_i\, q_i(t)$. The main benefit of choosing this particular basis is that it can be computed from a classical elastic mechanical problem, whereas open-circuit modes depend also on the piezoelectric system properties. As a result, the problem consists in solving the following coupled system [8, 18]

$$\begin{cases}\ddot{q}_i + 2\xi_i\omega_i\dot{q}_i + \omega_i^2 q_i + \sum_{p=1}^{P}\chi_i^{(p)}V^{(p)} = F_i, & \forall i \in \{1\dots N\},\\ C^{(p)}V^{(p)} - Q^{(p)} - \sum_{i=1}^{N}\chi_i^{(p)}\, q_i = 0, & \forall p \in \{1\dots P\},\end{cases} \tag{15}$$

with $F_i = \mathbf{\Phi}_i^{\mathrm{T}}\mathbf{F}$ the forcing of the i-th mode and $\chi_i^{(p)}$ the coupling coefficient associated to the i-th mode and the p-th patch, defined by

$$\left(\chi_i^{(1)}\,\chi_i^{(2)}\cdots\chi_i^{(P)}\right) = \mathbf{\Phi}_i^{\mathrm{T}}\mathbf{K}_c, \quad \forall i \in \{1\dots N\}. \tag{16}$$

These modal coupling coefficients $\chi_i^{(p)}$ are related to the MEMCF, denoted $k_i^{(p)}$, [3,8,17,18], which characterize, for each mode i, energy exchange between the mechanical structure and the piezoelectric patch p

$$k_i^{(p)} = \frac{\chi_i^{(p)}}{\sqrt{C^{(p)}}\omega_i}. \tag{17}$$

Under the assumption the modal truncation to one mode is valid around the i-th mode, one can obtains an approximation of the well known effective electromechanical coupling factor (EEMCF), denoted $k_{\mathrm{eff},i}$ by the following relation given in [8]

$$k_{\mathrm{eff},i}^2 = \frac{\hat{\omega}_i^2 - \omega_i^2}{\omega_i^2} \simeq \sum_{p=1}^{P}\left(k_i^{(p)}\right)^2, \tag{18}$$

with $\hat{\omega}_i$ the open-circuit angular frequency.

To summarize, the initial finite element formulation given by Eq. (10) has been replaced by the modal formulation Eq. (15), whose unknowns are the N modal coordinates q_i and the P voltage/charge pairs $\left(V^{(p)}, Q^{(p)}\right)$ associated with the P piezoelectric patches. Its major interest is the computation of the coupling parameters requires only a single modal analysis of the elastic problem. This operation can be done by any standard finite element code. Then, the MEMCF can be calculated from Eq. (17)

if one is able to compute the electromechanical coupling matrix for curved patches.

The most important parameter of the study is $k_i^{(p)}$ because the electrical components of the shunt only depend on it [8]. Then, it is proportional to the fraction of the system modal energy which is converted into electrical energy by the p-th open-circuit piezoelectric patch. As such, it is a direct measurement of the influence of the piezoelectric patch on the system.

3 THE ELECTROMECHANICAL COUPLING MATRIX

In the electromechanical coupling matrix definition (Eq. (6)), the quantities $e_{kij}n_k$ and ε_{ij} are expressed in the global frame of the system. However, it is more convenient, as shown below, to compute $\mathbf{K}_c$ in the local frame of the piezoelectric patch. A curved patch polarized in the normal direction (Fig. 1) is considered here. Henceforth, the indices i,

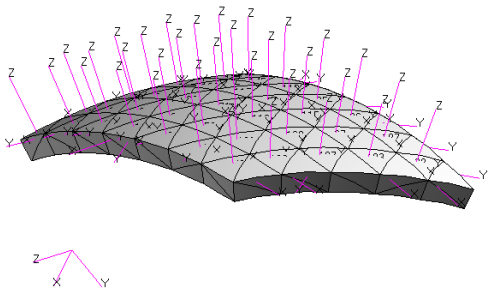

FIGURE 1. DISCRETIZED CURVED PATCH

j and k refer to the three directions of a frame attached to the piezoelectric patch and varying along it. Direction k is oriented according to the patch direction of polarization. Moreover, a_{ij} is defined as the transformation matrix (size 3×3) between the global and the local frame. Therefore, the equation (6) can be recasted as follows

$$\sum_{p=1}^{P} \frac{V^{(p)}}{h^{(p)}} \int_{\Omega^{(p)}} e_{kij} n_k a_{pi} a_{qj} \varepsilon_{pq} \left(\delta u\right) \mathrm{d}\Omega \quad \Longrightarrow \quad \delta \mathbf{U}^{\mathrm{T}} \mathbf{K}_c \mathbf{V}, \tag{19}$$

where $a_{pi}a_{qj}\varepsilon_{pq}$ is the strain tensor expressed in the local frame. The reason for having chosen the local frame comes from $e_{kij}n_k$ has a very simple expression while computed in it. According to the fact the piezoelectric material is transverse isotropic, and using Voigt notation, we have

$$\mathbf{e} = e_{k\alpha} n_k = \left(e_{31}\ e_{31}\ e_{33}\ 0\ 0\ 0\right)^{\mathrm{T}} \text{ with } \alpha = 1, \ldots, 6, \tag{20}$$

$\mathbf{e}$ is the vector of piezoelectric constants. In the same way, the discretized gradient operator $\mathbf{B}$, expressed in the global frame, and the transformation matrix $\mathbf{M}$ (size 6×6) applied to $\mathbf{B}$, are introduced. The classical discretization scheme allow writing $\boldsymbol{\varepsilon}_\alpha = \mathbf{Du} = \mathbf{DNU} = \mathbf{BU}$. The gradient operator and the interpolation functions matrix are denoted, respectively, $\mathbf{D}$ and $\mathbf{N}$. Consequently, the elementary electromechanical coupling matrix for the p-th patch is given by

$$\mathbf{K}_c^e = \frac{1}{h^{(p)}} \int_{\Omega_e} \mathbf{e}^{\mathrm{T}} \mathbf{M}^{\mathrm{T}} \mathbf{B}\, \mathrm{d}\Omega, \tag{21}$$

with Ω_e the volume of the finite element e. For the numerical applications, a quadratic tetrahedral element (TET10) was used. Four Gauss points allow to approximate $\mathbf{K}_c^e$ by

$$\mathbf{K}_c^e = \frac{1}{h^{(p)}} \mathbf{e}^{\mathrm{T}} \mathbf{M}^{\mathrm{T}} \left(\frac{1}{4} \sum_{i=1}^{4} \mathbf{B}_i \right) \Omega^e, \tag{22}$$

noting $\mathbf{B}_i$ the matrix $\mathbf{B}$ evaluated at the i-th Gauss point.

In order to validate the coupling matrix calculation method in 3D, a cantilever beam partially covered with 2 collocated piezoelectric patches, polarized in opposite directions, has been modeled with TET10 finite elements [19]. The EEMCF values, approximated by equation (18) for the first three bending modes (1B, 2B and 3B), are then compared to those coming from a 1D finite element model and to experimental measurements [8]. The short and open-circuit relative errors are listed in the table 1 and the EEMCF relative errors are given in the table 2. The EEMCF

	short-circuit freq.		open-circuit freq.	
Modes	$\Delta f_i/f_i^{\mathrm{1D}}$	$\Delta f_i/f_i^{\mathrm{exp.}}$	$\Delta \hat{f}_i/\hat{f}_i^{\mathrm{1D}}$	$\Delta \hat{f}_i/\hat{f}_i^{\mathrm{exp.}}$
1B	0.61%	5.44%	0.89%	5.77%
2B	0.42%	-0.08%	0.71%	0.07%
3B	0.22%	2.47%	0.43%	-2.68%

TABLE 1. 3D FE SHORT AND OPEN-CIRCUIT FREQUENCIES RELATIVE ERRORS COMPARED TO THE 1D MODEL AND THE EXPERIMENTAL MEASUREMENTS

relative error between 3D FE and 1D models is around 14% for the three modes. Although this is a relatively large error, it can be seen this error does not come from the fact that the 3D model is false but from the fact that a very small deviation of 0.5% on the open and short-circuit frequencies causes an EEMCF relative error of approximately 15%. The good agreement between 1D and 3D FE and between experimental results and 3D FE, with regards to the short and open-circuit frequencies, allows to validate the finite element developments.

	EEMCF	
Modes	$\Delta k_{\text{eff}}/k_{\text{eff}}^{\text{1D}}$	$\Delta k_{\text{eff}}/k_{\text{eff}}^{\text{exp.}}$
1B	16.06%	19.58%
2B	14.48%	8.82%
3B	13.14%	-19.00%

TABLE 2. 3D EEMCF RELATIVE ERRORS

4 OPTIMIZATION

The case of a single piezoelectric patch is considered in the rest of the study, for this reason the superscript p is omitted.

Since the size and location of the piezoelectric patch strongly influence the vibration reduction performance [16, 20], the mechanical optimization is of primary importance. More precisely, finding the design of a patch that maximize k_i is a combinatorial optimization problem. Such problem is characterized by search space growing exponentially with the number of configurations. In order to approach the optimum design in a reasonable amount of time, the mechanical optimization is split up into two steps.

4.1 FE Model and Parameterization

Some practical restrictions are made on the FE model characteristics in order to simplify the problem (Fig. 2): the meshes of the structure and the patch have to be compatible, the mesh of the structure is fixed (it won't be remeshed in the optimization procedure) and have to be regular, and the patch is rectangular. The size and location of one patch is entirely determined through 5 parameters: 2 curvilinear coordinates, denoted x_- and y_- for the location on the outer surface of the structure and 3 geometric parameters, denoted L_x, L_y and h. The figure 2 defines the new parameters notations. The patch is allowed to move inside an area defined by the user which corresponds in the figure 2 to the fine mesh zone. Hence, the number of values the parameters x_-, y_-, L_x and L_y can take is limited by the quality of the mesh. Therefore, the search space, denoted A, is a discrete and finite subset of $\mathbb{R}^5$ and the elements of A, denoted D, are called feasible solutions or designs here (Eq. (23)).

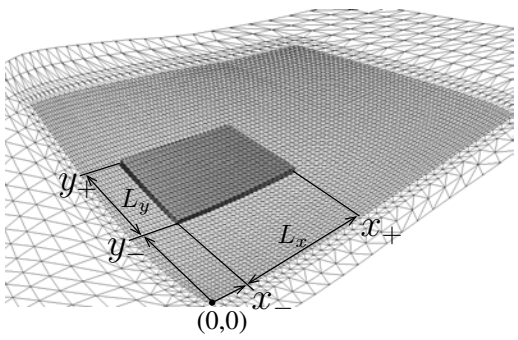

FIGURE 2. PATCH PARAMETERS

$$D = \{x_-, y_-, L_x, L_y, h\}. \tag{23}$$

4.2 First Step of the Optimization Procedure

The main idea is to derive a modal coupling indicator from the plate analytical theory and to use it for the 3D problem with an assumption consisting to say slightly curved patch modal coupling is roughly the same whether the curvature is taken into account or not.

4.2.1 Coupling Indicator Derivation

The differential equation for transverse motion of a plate with a flat piezoelectric patch bonded onto its surface is given by [21]

$$D_p \Delta\Delta w + \Delta M_p + \rho_p h_p \ddot{w} = q. \tag{24}$$

D_p is the bending stiffness of the plate, w the transverse displacement, ρ_p and h_p are the plate density and thickness and q the externally applied transverse force. Δ is the Laplacian operator and M_p is the moment term coming from the forces exerted by the piezoelectric patch. The equation (24) is derived from the Kirchhoff-Love plate theory where the transverse shear stress and rotational inertia are neglected.

In the case of an uniformly polarized flat rectangular piezoelectric patch, the moment term M_p is given by

$$M_p = \Theta \left[\mathrm{H}(x - x_-) - \mathrm{H}(x - x_+)\right] \left[\mathrm{H}(y - y_-) - \mathrm{H}(y - y_+)\right) \; V, \tag{25}$$

where Θ is a constant that depends on stiffness parameters and the piezoelectric constant e_{31} and the potential difference V. The Heavyside function H and the coordinates x_-, x_+, y_- and y_+ are used to describe the spatial footprint of the patch in the directions $\mathbf{x}$ and $\mathbf{y}$. To introduce the modal coupling indicator, the transverse displacement w is expanded onto the transverse normal modes basis of the plate (ψ_i, ω_i)

$$w(x, y, t) = \sum_{i=1}^{\infty} \psi_i(x, y) q_i(t). \tag{26}$$

By injecting Eq. (26) in Eq. (24) and using the orthogonality properties of the modes, one obtains

$$\ddot{q}_i + 2\xi_i \omega_i \dot{q}_i + \tilde{k}_i V + \omega_i^2 q_i = q_i \quad i \in \mathbb{N}, \tag{27}$$

with

$$\tilde{k}_i = \iint_S \Delta M_p \, \psi_i \, \mathrm{d}S, \tag{28}$$

where S is the surface of the piezoelectric patch footprint. If the plate is discretized with 3D finite elements, then the transverse modal displacement $\psi_i(x, y)$ at each node can be obtained by computing the scalar product between the finite element eigenmodes $\mathbf{\Phi}_i$ (computed with Nastran for example, size $N \times 1$, with N the dof number) and the normal vectors to the surface at each node, denoted $\mathbf{n}$. As a result, on can rewrite $\tilde{k}_i$ as

$$\tilde{k}_i = \iint_S \Delta M_p \, (\mathbf{\Phi}_i.\mathbf{n}) \, \mathrm{d}S. \tag{29}$$

Inserting Eq. (25) in Eq. (29) leads to the following developed expression of $\tilde{k}_i$

$$\begin{aligned} \tilde{k}_i = \Theta \int_{x_-}^{x_+} \left(\frac{\partial \left(\Phi_i.\mathbf{n}\right)}{\partial y}_{|y=y_+} - \frac{\partial \left(\Phi_i.\mathbf{n}\right)}{\partial y}_{|y=y_-} \right) \mathrm{d}x \\ + \Theta \int_{y_-}^{y_+} \left(\frac{\partial \left(\Phi_i.\mathbf{n}\right)}{\partial x}_{|x=x_+} - \frac{\partial \left(\Phi_i.\mathbf{n}\right)}{\partial x}_{|x=x_-} \right) \mathrm{d}y. \end{aligned} \tag{30}$$

$\tilde{k}_i$ is the coupling coefficient within the frame of the plate theory. It depends only on the patch geometric parameters x_-, x_+, y_- and y_+, the modes $\mathbf{\Phi}_i$ and a constant parameter Θ. The constant has no importance since the purpose is to study the variations of $\tilde{k}_i$ according to the patch design. Thus, the goal is to find four out of the five design parameters that maximize $\tilde{k}_i$. At last, only one normal computation is required since the coupling indicator works with the modes of the naked structure.

4.2.2 Simulated Annealing Algorithm

For the fan blade application and according to its mesh refinement, the order of magnitude is 10^{5p} feasible designs for p patches. Thus, using exhaustive enumeration to find the better design is an unpracticable method. In the hope of obtaining a more efficient procedure to solve this combinatorial optimization problem, the simulated annealing (SA) algorithm is adopted. It is a probabilistic metaheuristic commonly used when the search space is discrete [9–11, 22, 23]. The goal is to find a good approximation to the global minimum of a cost function, denoted C_i. A simple cost function, which quantify the performance of a piezoelectric patch for the i-th mode, can be defined by

$$C_i = -\tilde{k}_i^2, \tag{31}$$

with $\tilde{k}_i$ defined by Eq. (30). By analogy with the annealing process, each step of the SA algorithm replaces the current design by a random neighbor design, chosen with a probability that depends on a global parameter T (called the temperature), that is gradually decreased during the process. The dependency is such that the current design changes almost randomly when T is large, but increasingly local as T goes to zero. The new generated designs are then evaluated and submitted to an acceptance test. If the cost function has to be minimized, transformations with cost decrement are always accepted while transformations increasing the cost are accepted according to a probability based on Boltzmann factor. The probabilistic nature of SA allows it to temporally accept worse solutions to escape from local minima. For further explanations and details about the SA algorithm, we refer the reader to [24]. In spite of the SA success [15], the algorithm demands a careful adjustment of the annealing schedule to achieve high performance in solving a combinatorial optimization problem. Therefore, a version of the SA called Thermodynamic Simulated Annealing (TSA) was chosen to perform the numerical simulations. Its main advantage is the temperature drop (cooling schedule) is not externally controlled by the user but continuously computed from the measurement of state functions variation (cost function variation). The TSA algorithm is detailed in [9] and its output is a design D as defined by Eq. (23).

4.2.3 Working Schedule of the First Step

From a practical point of view, defining the design of a piezoelectric patch (4 parameters in the first step) is equivalent to select a number of finite elements belonging both to the area inside which the patch is allowed to move and to the patch footprint. The values of the mode at the nodes located at the patch boundary are then used to derive $\tilde{k}_i$ and so C_i. All these calculations are very fast with Matlab and allow testing a huge number of design (one modal analysis only). As shown in the figure 3, a loop on the TSA algorithm is applied to generate several "good" starting designs for the second step of the optimization procedure.

4.3 Second Step of the Optimization Procedure

The main hypothesis of the first part is now released and the new problem is to perform an optimization when the mass and the stiffness of the patch are taken into account. It means to compute the eigenmodes problem Eq. (14) for each new tested design. Solving Eq. (14) is time consuming for an industrial FE mesh and cannot be done more than few thousand times in a reasonable amount of time. Consequently, the idea is to start the search from good solutions (coming from the TSA algorithm) to avoid testing too many designs before reaching a configuration that minimize the cost function. The purpose is now to look after the influence of patch's mass and stiffness on the optimal design found previously. In other word, one has to find the five design parameters that minimize the following new cost function

$$C_i = -k_i^2. \tag{32}$$

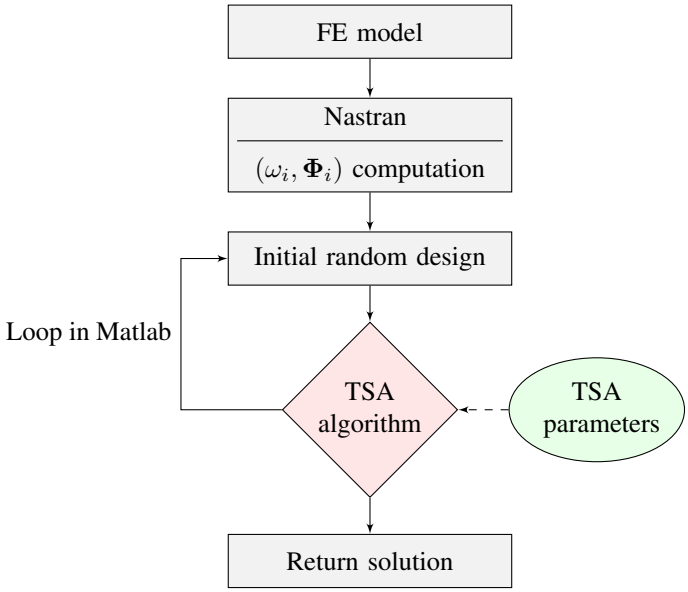

FIGURE 3. WORKING SCHEDULE, FIRST STEP

Where k_i is defined by Eq. (17). To achieve this goal, a tabu search algorithm [13,25] is chosen. It is a local search technique using a memory structure to enhance the performance of local search method.

4.3.1 Tabu Search With a tabu search, the movement through search space (*i.e.* the set of feasible designs) is via local neighborhoods of the current design.

For a design $D = \{a_i\}$, $i = (1, 2, ..., \lambda)$, with $\lambda = 5$ (Eq. (23)). A neighborhood of D, denoted $N(D)$, is considered here to be the following set of designs [13]

$$N(D) = \{D_i\} \quad i = 1, \cdots, 2\lambda, \tag{33}$$

where, if $a_j = s_k$ with $k \in (1, 2, \cdots, m)$, m ranging depending on whether s_k is a particular design variable, then, for $j = (1, \cdots, \lambda)$

$$D_j = \{a_1, \cdots, a_{j-1}, s_{k-1}, a_{j+1}, \cdots, a_\lambda\}, \tag{34}$$

and again for $j = 1, 2, \cdots, \lambda$

$$D_{j+\lambda} = \{a_1, \cdots, a_{j-1}, s_{k+1}, a_{j+1}, \cdots, a_\lambda\}, \tag{35}$$

with $k \pm 1$ modulo $m \in (1, 2, \cdots, m)$. The neighborhood expressed by Eq. (33), with design given by equations Eq. (34) and Eq. (35) is considered to have depth 1. To broaden the neighborhood to a depth β, s_{k-1} and s_{k+1} are replaced by $s_{k-\beta}$ and $s_{k-\beta}$. Hence, a β-depth neighborhood is such that $i = 1, 2, \cdots, 2\beta\lambda$. If D is the current design and $N(D)$ its neighborhood, then the search moves to the allowed design D' in N(D) with the highest MEMCF. D' is allowed if it does not belong to the tabu list. The latter is a one-dimensional array which acts as a short-term memory in that it contains a specific number (tabu length) of the most recently accepted designs. Once the search has moved to D', it is included in the tabu list. The procedure of generating a neighborhood, accepting the allowed design and then updating the tabu list is the most basic tabu search technique and may be repeated until a maximum number of iterations is reached or a specified computation time is exceeded. A merit of the tabu list is the prevention, to a degree, of cycling within a small subset of the search space [13]. A detailed description of the tabu search can be found in [25, 26].

Nonetheless, as we start the tabu search with a "good" design, the depth of the neighborhood is set to one because the purpose is to optimize locally the design. This second step of the optimization procedure is performed as follows.

1. creation of $N(D)$ from a starting design
2. structural eigenmodes computation thanks to Nastran for all the designs belonging to the neighborhood
3. selection of the better allowed design ($D' \rightarrow D$)
4. loop on the first step of the algorithm.

4.3.2 Working Schedule of the Second Step As viewed above, the only time consuming operation is the computation of the short-circuit eigenmodes $(\omega_i, \mathbf{\Phi}_i)$. This step, mandatory to calculate the MEMCF, is done with the commercial finite element analysis program Nastran. It is a widely used software in the industry and is efficient for eigenmodes computation of large systems (several tens of thousands dofs). Some technical difficulties have to be overcomed to realize the second step of the tabu search:

1. create the volumic mesh of the patch on the outer surface of a 3D structure,
2. associate to each finite element belonging to a piezoelectric patch a local frame oriented according to its direction of polarization,
3. compute $\mathbf{K}_c$ and then k_i,
4. loop the procedure for the set of designs (the neighborhood)

The calculation procedure used to evaluate k_i for each design is shown schematically in the diagram Fig. 4. The Matlab software is exploited here as a shell to manage Patran and Nastran. For each new design, the patch mesh is recreated with Patran and a new normal mode computation is launched with Nastran. Throughout the procedure, much information is exchanged between Matlab, Patran and Nastran, for this reason, the programming language Awk is used because it allows reading and writing very fast. The assembly of $\mathbf{M}$ and $\mathbf{K}_c$ and the computations of

the MEMCF and the frequency response function (FRF) are the only operations done in Matlab. The main requirement to be able

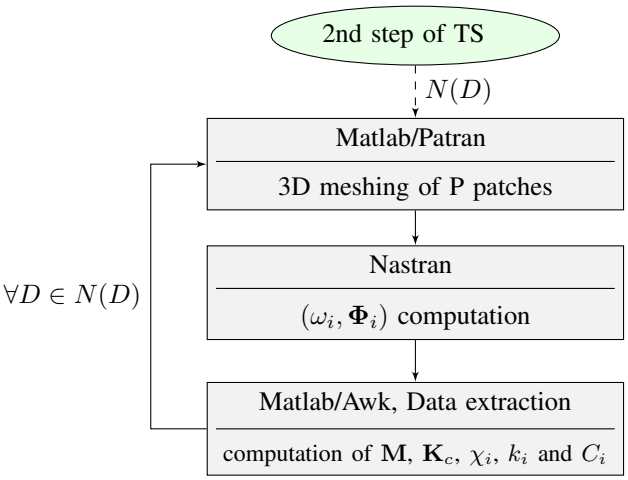

FIGURE 4. 2nd STEP OF THE TABU SEARCH

to deal with hundreds simulations is to cut back the time passed out of Nastran. Some results about the performance of the working schedule (Fig. 4) are summarized in Tab. 3.

	Time used by Nastran / Total time		
patches	10^3 dofs	10^4 dofs	10^5 dofs
2	98	96	91
4	98	95	91

TABLE 3. TIME RATIOS [%]

5 APPLICATION TO A TURBOJET FAN BLADE

The fan blade used for the numerical simulations is a structure of approximately 560 mm×250 mm×7 mm for a weigth of 4.86 kg. It is discretized with 21,616 TET10 elements which correspond to 124,614 dofs. The targeted modes are the first free-free bending mode (1B, 132 Hz), the second bending mode (2B, 350 Hz) and the first torsion mode (1T, 512 Hz).

5.1 Validation of the Optimization Procedure

Despite the brute-force search (exhaustive enumeration) is not the right method, it is useful to benchmark an optimization algorithm on a search space of manageable size. Therefore, to validate the optimization procedure exposed above, the search space is limited to three design parameters (x_-, y_- and h): one piezoelectric patch with its length and width fixed (100×60 mm). The

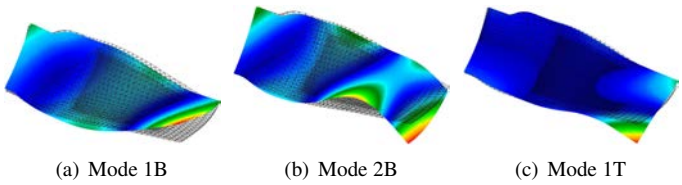

(a) Mode 1B (b) Mode 2B (c) Mode 1T

FIGURE 5. FREE-FREE MODES SHAPES

result produced by the exhaustive search method is then compared to the one coming from the optimization procedure.

5.1.1 Exhaustive Search In order to find the better design, a path is applied to the patch so that it scans the entire area that was bounded. Given the size of the patch, 195 different locations are explored and six thicknesses (0.5, 1, 2, 3, 4 and 5 mm) are tested for each of them. The exhaustive search leads to solve 1170 eigenvalue problems for a CPU time around 18 hours. The results for the first bending mode are shown in the figure 6. The k_1 (MEMCF for the mode 1B) value corresponding to the

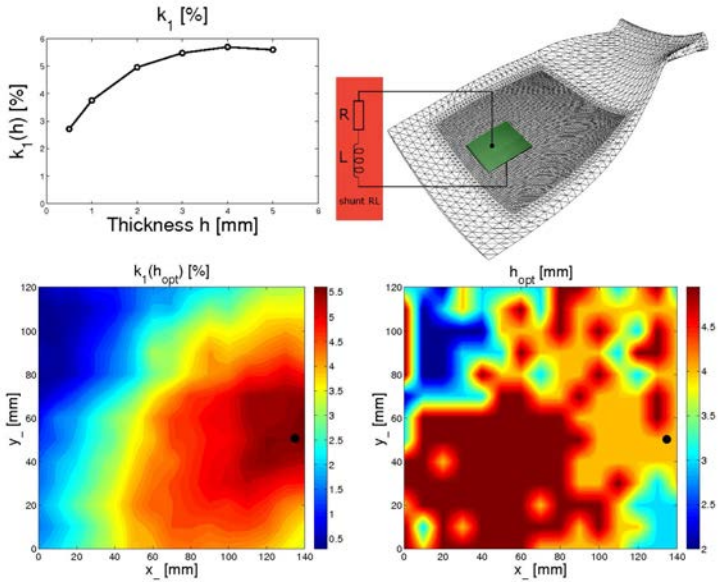

FIGURE 6. EXHAUSTIVE SEARCH RESULTS FOR THE 1B

optimal thickness h_{opt} is plotted for each position. A black dot indicates the best location. It can be noticed that computing the optimal value for the thickness h is of major importance, since $h_{\text{opt}} = 4$ mm for this position leads to double k_1, as compared to $h = 0.5$ mm. The so determined patch, of mass that represents 3% of the total fan mass, has a MEMCF of 5.5%. The placement and optimal thickness are also calculated for the modes 2B and 1T.

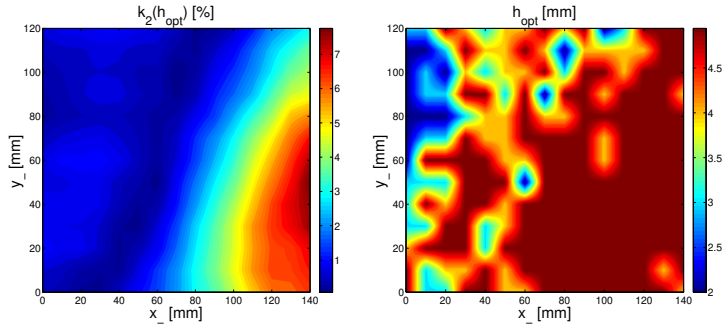

(a) Mode 2B

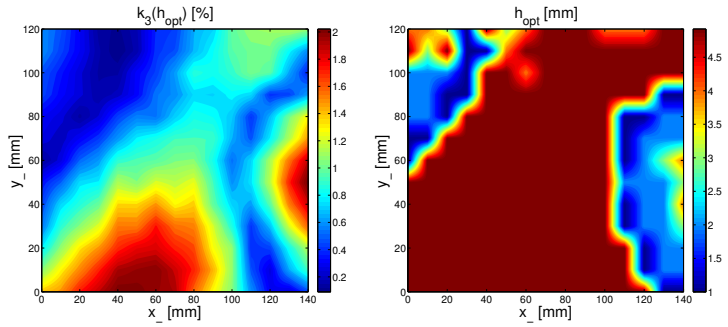

(b) Mode 1T

FIGURE 7. EXHAUSTIVE SEARCH RESULTS

5.1.2 Optimization Algorithms The optimization procedure leads to the same optimal location and optimal thickness but the CPU time is reduced to around half an hour per targeted mode. If the mode 1B is considered (Fig.8), all the designs given by the TSA algorithm indicate a patch location in the area on the fan blade surface where the von Mises equivalent strain is maximum (patch with dashes). Then, the tabu search, starting with these designs, moves the patch along different locations and allows to find the optimal placement after approximately 40 eigenvalue problems resolutions.

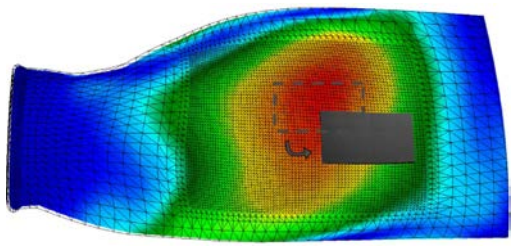

FIGURE 8. OPTIMIZATION ALGORITHMS RESULT, MODE 1B

Many other validation test can be conducted, as long as a reference solution can be found. In our case, given the large computational time, only one patch with 3 free parameters can be fully simulated and thus provide a reference solution.

5.2 Resonant Shunt Application

In this section, a resonant shunt is succesively connected on the piezoelectric patch determined for the modes 1B, 2B et 1T and tuned for each of them. When the modes are quite distinct from each other, the optimal electrical components of the resonant shunt are calculated directly from k_i and the frequency of the mode [3]. Moreover, if the modal damping ξ_i associated to each mode is known, the attenuation bring by the resonant shunt is a function of k_i [3]. The optimal electrical parameters and the corresponding estimated attenuation are given in the table 4. The values of L might seem very important, but they are

mode	k_i [%]	R [Ω]	L [H]	ξ	Att. [db]
1B	5.5	8429	136	10^{-4}	45
2B	8.0	4409	18	10^{-4}	50
1T	2.0	777	9	$6 \cdot 10^{-4}$	20

TABLE 4. EXPECTED ATTENUATION

easily attainable using a simulated inductor (gyrator). If a gyrator is employed then the system becomes semi-passive (electric supply) but remains unconditionally stable since no energy is injected into the structure. Finally, the frequency response functions (FRF) for the three modes are computed with a modal basis truncated to the first ten modes. An harmonic forcing is applied at the tip of the fan blade and the driving point FRF modulus are plot at the same point.

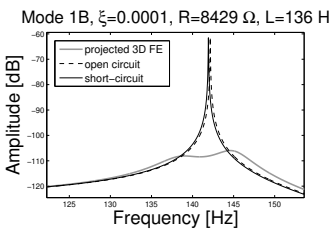

(a) Mode 1B

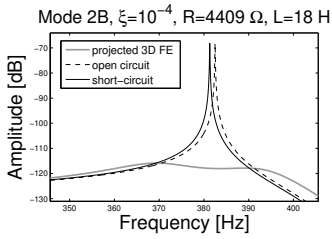

(b) Mode 2B

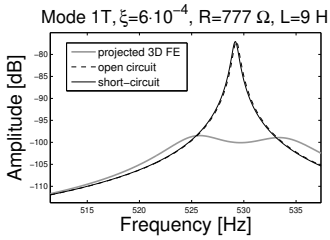

(c) Mode 1T

FIGURE 9. FAN BLADE TIP FRF

6 CONCLUSION

This study presents three novel aspects. The first one is the use of an original FE model to solve the electromechanical problem of an industrial complex structure equipped with a piezoelectric patch. The second is the decomposition of the mechanical optimization in two steps in order to have a less expensive computation time. At last, it is the derivation of an analytic coupling indicator allowing to evaluate a huge number of patch design.

Three main results have to be stressed. The first one is the optimization procedure for one patch can be done on a 3D mesh of around 10^5 dofs within a reasonable time (30 min) if some optimization algorithms are used. Then the MEMCF is very sensitive to the thickness of the patch, which is an often overlooked parameter in the optimization procedure. Finally, it was shown that the additional stiffness provided by the patch modifies significantly the optimal position found at the end of the first optimization step.

The future work is about the experimental validation of the FE model on the fan blade itself. This validation will be conducted for the free-free boundary conditions but also for the clamped-free to approach the mechanical operating conditions. Then, the natural extension of this work is to apply the optimization procedure to the case of several patches but new problems arise like, for instance, the definition of a relevant cost function.

Lastly, it is important to mention this method is applied here to a resonant shunt but remains valid for a resistive shunt or switch techniques since the mechanical and electrical optimizations are uncoupled.

ACKNOWLEDGMENT

This work (Cifre thesis), in cooperation with Snecma, is a part of the joint research program MAIA supported by the CNRS, the ONERA and the SAFRAN group.

REFERENCES

[1] Hagood, N. W., and Flotow, A. V., 1991. "Damping of structural vibrations with piezoelectric materials and passive electrical networks". *Journal of Sound and Vibration,* ***146***(2), pp. 243–268.

[2] Richard, C., Guyomar, D., Audigier, D., and Bassaler, H., 2000. "Enhanced semi-passive damping using continuous switching of a piezoelectric device on an inductor". In Smart Structures ans Materials : Passive Damping and Isolation, SPIE, Vol. 3989, pp. 288–299.

[3] Ducarne, J., 2009. "Modelization and optimization of non-linear structural damping devices with piezoelectric switching shunts". PhD thesis, Structural Mechanics and Coupled Systems Lab., Cnam, France.

[4] Davis, C. L., and Lesieutre, G. A., 1995. "A modal strain energy approach to the prediction of resistively shunted piezoceramic damping". *Journal of Sound and Vibration,* ***184***(1), pp. 129–139.

[5] Becker, J., Fein, O., Maess, M., and Gaul, L., 2006. "Finite element-based analysis of shunted piezoelectric structures for vibration damping". *Computers and Structures,* ***84***(31-32), pp. 2340–2350.

[6] Ducarne, J., Thomas, O., and Deü, J.-F., 2007. "Optimisation de dispositif passif d'attnuation de vibration par shunt pizolectrique". In Actes du 8ème colloque national en calcul de structures, Vol. 2, Hermes, pp. 519–524. In french.

[7] Ducarne, J., Thomas, O., and Deü, J.-F., 2009. "Performance and optimization of piezoelectric shunts for vibration reduction". *Journal of Sound and Vibration*. In preparation.

[8] Thomas, O., Deü, J.-F., and Ducarne, J., 2009. "Vibration of an elastic structure with shunted piezolectric patches: Efficient finite element formulation and electromechanical coupling coefficients". *International Journal for Numerical Methods in Engineering,* ***80***.

[9] de Vicente, J., Lanchares, J., and Hermida, R., 2003. "Placement by thermodynamic simulated annealing". *Physics Letters A,* ***317***(5-6), pp. 415–423.

[10] Duque-Antón, M., 1997. "Constructing efficient simulated annealing algorithms". *Discrete Applied Mathematics,* ***77***, pp. 139–159.

[11] Fabian, V., 1997. "Simulated annealing simulated". *Computers & Mathematics with Applications,* ***33***(1/2), pp. 81–94.

[12] Zheng, C., and Wangb, P., 1996. "Parameter structure identification using tabu search and simulated annealing". *Advances in Water Ressources,* ***19***(4), pp. 215–224.

[13] Bland, J. A., 1995. "Discrete-variable optimal design using a tabu search approach". *The Built Environment, Wit Press,* ***13***, pp. 415–423.

[14] Michel, L., and Hentenryck, P. V., 2004. "A simple tabu search for warehouse location". *European Journal of Operational Research,* ***157***, pp. 576–591.

[15] Jr, M. A. A., Kadipasaoglub, S. N., and Khumawalab, B. M., 2006. "An empirical comparison of tabu search, simulated annealing, and genetic algorithms for facilities location problems". *International Journal Production Economics,* ***103***, pp. 742–754.

[16] Belloli, A., and Ermanni, P., 2007. "Optimum placement of piezoelectric ceramic modules for vibration suppression of highly constrained structures". *Smart Materials and Structures,* ***16***.

[17] Anderson, E. H., and Hagood, N. W., 1992. "Simultaneous piezoelectric sensing / actuation : analysis and application to controlled structures". *Journal of Sound and Vibration,* ***174***(5), pp. 617–639.

[18] Porfiri, M., Maurini, C., and Pouget, J., 2007. "Identification of electromechanical modal parameters of linear piezoelectric structures". *Smart Materials and Structures,* ***16***.

[19] Sénéchal, A., Thomas, O., and Deü, J.-F., 2009. "Atténuation des vibrations de structures complexes par shunt piézoélectrique - application un modèle simplifié d'aube de turbomachine". In Actes du 9ème colloque national en calcul de structures, Vol. 2, Hermes, pp. 707–712. In french.

[20] Frecker, M. I., 2003. "Recent advances in optimization of smart structures and actuators". *Journal of Intelligent Systems and Structures,* ***14***(4-5), pp. 207–216.

[21] Sonti, V. R., Kim, S. J., and Jones, J. D., 1995. "Equivalent forces and wavenumber spectra of shaped piezoelectric actuators". *Journal of Sound and Vibration,* ***187***(1), pp. 111–131.

[22] Moita, J. M. S., Correia, V. M. F., and *al*, 2006. "Optimal design in vibration control of adaptive structures using a simulated annealing algorithm". *Composite Structures,* ***75***, pp. 79–87.

[23] Correia, V. M. F., Soares, C. M. M., and Soares, C. A. M., 2001. "Refined models for the optimal design of adaptive structures using simulated annealing". *Composites Structures,* ***54***, pp. 161–167.

[24] S. Kirkpatrick, C. D. G., and Vecchi, M. P., 1983. "Optimization by simulated annealing". *Science,* ***200***(4598).

[25] Glover, F., 1989. "Tabu search - part 1". *ORSA Journal on Computing,* ***1***, pp. 190–206.

[26] Glover, F., 1990. "Tabu search - part 2". *ORSA Journal on Computing,* ***2***, pp. 4–32.